A STUDY ON THE ROLE OF GRAIN-BOUNDARY ENGINEERING IN PROMOTING HIGH-CYCLE FATIGUE RESISTANCE AND IMPROVING RELIABILITY IN METALLIC ALLOYS FOR PROPULSION SYSTEMS

FINAL REPORT

AFOSR Grant no. F49620-02-1-0010

Robert O. Ritchie[1] and Mukul Kumar[2]

[1]Department of Materials Science and Engineering, University of California at Berkeley
[2]Lawrence Livermore National Laboratory

Foreword

This research program, on "A study of the role of grain-boundary engineering in promoting high-cycle fatigue resistance and improving reliability in metallic alloys for propulsion systems", was supported by the Air Force Office of Scientific Research between December 1, 2001, and May 31, 2005, under AFOSR Grant no. F49620-02-1-0010, with Professor Robert O. Ritchie, of the University of California, Berkeley, as principal investigator, and Dr. Mukul Kumar, of the Lawrence Livermore National Laboratory, as co-principal investigator

Abstract

High-cycle fatigue, involving the premature initiation and/or rapid propagation of small cracks to failure due to high-frequency (vibratory) loading, remains the principal cause of failures in military gas-turbine propulsion systems. The objective of this study is to examine whether the resistance to high-cycle fatigue failures can be enhanced by grain-boundary engineering, i.e., through the modification of the spatial distribution and topology of the grain boundaries in the microstructure. While grain-boundary engineering has been used to obtain significant improvements in intergranular corrosion and cracking, creep and cavitation behavior, toughness and plasticity, cold-work embrittlement, and weldability, only very limited, but positive, results exist for fatigue. Accordingly, using a Ni-base γ/γ' superalloy, René 104 (also referred to as ME3), as a typical engine disk material, sequential thermomechanical (cyclic strain and annealing) processing is used to (i) modify the proportion of special grain boundaries, and (ii) interrupt the connectivity of the random boundaries in the grain-boundary network. The processed microstructures are then subjected to high-cycle fatigue testing, first to assess the crack-propagation properties of long and small cracks to examine how the altered grain-boundary population and connectivity can influence growth rates and overall lifetimes.

Research objectives

Nickel-base superalloys are widely used in turbines for both aerospace and land-based power generation applications, due to their exceptional elevated-temperature strength, high resistance to creep, oxidation, corrosion, and good fracture toughness. However, a critical property of these alloys is their resistance to fatigue-crack propagation, particularly at service

REPORT DOCUMENTATION PAGE

Form Approved
OMB No. 0704-0188

1. REPORT DATE *(DD-MM-YYYY)*	2. REPORT TYPE	3. DATES COVERED *(From - To)*
	Final Report	01 November 2001 - 30 April 2005

4. TITLE AND SUBTITLE

A Study on the Role of Grain-Boundary Engineering in Promoting High-Cycle Fatigue Resistance and Improving Reliability in Metallic Alloys for Propulsion Systems

5a. CONTRACT NUMBER

5b. GRANT NUMBER

F49620-02-1-0010

5c. PROGRAM ELEMENT NUMBER

6. AUTHOR(S)

Robert O. Ritchie

5d. PROJECT NUMBER

5e. TASK NUMBER

5f. WORK UNIT NUMBER

7. PERFORMING ORGANIZATION NAME(S) AND ADDRESS(ES)

Department of Materials Science and Engineering
University of California at Berkeley

8. PERFORMING ORGANIZATION REPORT NUMBER

9. SPONSORING/MONITORING AGENCY NAME(S) AND ADDRESS(ES)

USAF/AFRL
AFOSR
875 North Randolph Street
Arlington VA 22203

Brett Conner/NA

10. SPONSOR/MONITOR'S ACRONYM(S)

AFOSR

11. SPONSOR/MONITOR'S REPORT

AFRL-SR-AR-TR-06-0444

12. DISTRIBUTION/AVAILABILITY STATEMENT

Distribution Statement A. Approved for public release; distribution is unlimited.

13. SUPPLEMENTARY NOTES

14. ABSTRACT

High-cycle fatigue, involving the premature initiation and/or rapid propagation of small cracks to failure due to high-frequency (vibratory) loading, remains the principal cause of failures in military gas-turbine propulsion systems. The objective of this study is to examine whether the resistance to high-cycle fatigue failures can be enhanced by grain-boundary engineering, i.e., through the modification of the spatial distribution and topology of the grain boundaries in the microstructure. While grain-boundary engineering has been used to obtain significant improvements in intergranular corrosion and cracking, creep and cavitation behavior, toughness and plasticity, cold-work embrittlement, and weldability, only very limited, but positive, results exist for fatigue. Accordingly, using a Ni-base y/y superalloy, Rene 104 (also referred to as ME3), as a typical engine disk material, sequential thermomechanical (cyclic strain and annealing) processing is ued to (i) modify the proportion of special grain boundaries, and (ii) interrupt the connectivity of the random boundaries in the grain-boundary network. The processed microstructures are then subjected to high-cycle fatigue testing, first to assess the crack-propagation properties of long and small cracks to examine how the altered grain-boundary population and connectivity can influence growth rates and overall lifetimes.

15. SUBJECT TERMS

16. SECURITY CLASSIFICATION OF:			17. LIMITATION OF ABSTRACT	18. NUMBER OF PAGES	19a. NAME OF RESPONSIBLE PERSON
a. REPORT	b. ABSTRACT	c. THIS PAGE			19b. TELEPHONE NUMBER *(Include area code)*
U	U	U	UU	32	

temperatures. In engine applications, there are often two components to this problem: (i) low-cycle fatigue, which results from relatively large cycles associated with the stopping and starting of the turbine, and (ii) high-cycle fatigue, associated with vibrational loading during service. High-cycle fatigue (HCF) in particular has been recognized as the single largest cause of engine failures in military aircraft.[1] It results in rapid, and often unpredictable, failures due to the propagation of fatigue cracks in blade and disk components under high-frequency loading, where the cracking initiates from small defects, in many instances resulting from fretting or foreign-object damage.[2] Due to the high vibrational frequencies involved, even cracks growing at slow per-cycle velocities can propagate to failure in short time periods, possibly within a single flight segment. Consequently, HCF-critical turbine-engine components must be operated below the fatigue-crack initiation or growth thresholds such that cracking cannot occur within ~10^9 cycles. To address this problem, significant research efforts have been directed in recent years to developing HCF design and life-prediction methodologies for titanium- and nickel-base alloys; these studies have resulted in an extensive database on HCF,[1,3,4] which has been exclusively directed to typical blade and disk microstructures.[5-8] However, the question as to whether these microstructures can be optimized to promote HCF resistance has rarely been addressed.

One approach to enhancing microstructural resistance to fracture has been through the notion of grain-boundary engineering, where the "character" of the grain boundaries is changed by thermomechanical treatment.[9] Specifically, the grain-boundary character distribution (GBCD) is controlled principally by promoting a high proportion of so-called "special" grain boundaries. These boundaries are characterized by a particular misorientation and high degree of atomic matching; they are described geometrically by a low "sigma number", Σ ($1<\Sigma\leq 29$), which is defined in terms of the coincident-site lattice (CSL) model [10] as the reciprocal of the fraction of lattice points in the boundaries that coincide between the two adjoining grains, with an allowable angular deviation from the Brandon criterion of $\Delta\theta \leq 15^\circ\cdot\Sigma^{-1/2}$.[11] Processing generally involves several strain-annealing cycles to induce (i) strain by cold working and (ii) strain-induced grain-boundary migration during subsequent annealing, the latter creating special grain boundaries via a boundary decomposition mechanism in the grain-boundary network.[12] In addition to an enhanced fraction of special boundaries, such "engineered" microstructures can possess a refined grain size and diminished incidence of deviation from the exact Σ misorientations; the texture, however, generally remains unchanged or, in some cases, can be reduced.

The aim of this project was to optimize microstructures using a thermomechanical processing approach in order to systematically modify the grain-boundary character distribution and boundary network topology. We evaluated the feasibility of this processing methodology for improving the HCF resistance of turbine-engine alloys, specifically by increasing the proportion of "special" grain boundaries in a polycrystalline Ni-base superalloy and by breaking-up the interconnected random grain-boundary network. The uniqueness of this approach is that it can alter the microstructural features in a controlled manner at dimensions relevant to the size of the propagating small cracks that are the essence of HCF failures.

Approach

Engineering of the grain-boundary microstructure in a material has been shown to be particularly successful in promoting resistance to specific modes of fracture, such as intergranular stress-corrosion cracking[13-20] and creep.[21-24] In general, this involves the use of thermomechanical processing to alter the misorientation distribution function (MDF), or the grain-boundary character distribution (GBCD), in order to increase the fraction of grain boundaries that exhibit special misorientations characterized by the coincident site lattice (CSL) model. Electron backscatter diffraction (EBSD) provides a convenient method to measure the special fraction and the GBCD, as well as the triple-junction distribution.

Precise mechanistic understanding about why such an increase in the fraction of special boundaries enables an improvement in the mechanical and chemical properties of low to medium stacking fault energy (SFE) FCC materials is still limited. However, studies[12-20] have indicated that the improvements in properties may be correlated with the connectivity of random boundary networks, but this has not been verified by direct observations.

Although grain-boundary engineering has been successful in promoting specific modes of fracture resistance, its effect on the fatigue resistance has largely been unexplored; indeed, to our knowledge, only one such study exists in archival literature.[25] In that study, ambient-temperature, smooth-bar, tension-tension fatigue lives for two γ/γ' superalloys were reported to be increased by a factor of ~1.5 in an Fe-base alloy by increasing the fraction of special boundaries from 20 to 65%, and by a factor of 3 in a Ni-base alloy by increasing this fraction from 9 to 49%, although no mechanistic explanation was presented.

Clearly the effectiveness of grain-boundary engineering will depend upon the nature of the crack path, specifically, the preponderance of intergranular vs. transgranular cracking. In light of this, the objective of the present study was to investigate, for the first time, the feasibility of using grain-boundary engineering processing to promote resistance to fatigue-crack propagation, particularly at near-threshold levels, in a new polycrystalline nickel-base disk alloy René 104 (also known as ME3). Specifically, crack-growth rates and threshold behavior of both large (8-20 mm) through-thickness cracks and small (~10-900 μm) surface cracks were examined; in the case of the large cracks over a range of temperatures from 25 to 800°C in order to enhance the incidence of intergranular crack growth.

In summary, our overall approach was to discern the feasibility of grain-boundary engineering techniques for optimizing microstructures for resistance to fatigue failure in a nickel-base superalloy, in particular involving high-cycle fatigue and the initiation and growth of long and small cracks, and in light of this to understand how cracks interact with grain boundaries of known crystallographic character.

Experimental procedures

Materials: Based on discussions with NASA Glenn and GE Aircraft Engines (GEAE), an advanced powder-metallurgy nickel-base superalloy, René 104 (also called ME3), was used in this study. It is a relatively new polycrystalline Ni-Co-Cr alloy, with a chemical composition similar to Udimet 720, which was designed to have extended durability at 650°C for aircraft engine disk applications by utilizing a moderately high γ' precipitate content with high

refractory element levels. Forged heats of the alloy were received as plate stock from GE Aircraft Engines (*fine-grain*) and NASA Glenn (*coarse-grain*). The as-received microstructure comprised a bimodal distribution of ~20 and 100-200 nm ordered γ' ($L1_2$) precipitates within the equiaxed γ matrix, as described by Nembach and Neite.[26] The matrix grain size, D_g, was 1.3 and 15 μm in the two as-received conditions for the GE and NASA heats, respectively. Typical ambient and elevated temperature mechanical properties are listed in Table I.[27]

Thermomechanical treatments: To vary the grain-boundary character distribution, the effects of several thermomechanical processing parameters were first evaluated, including pre-strain (by cold rolling), annealing time and temperature. Based on earlier grain-boundary engineering processing of Inconel 600,[24] cold rolling was used to vary the pre-strain from 5 to 20%, followed by annealing at temperatures from 1000° to 1170°C with annealing times of 15 to 45 min; in addition, air cooling instead of water or oil quenching was adopted to avoid quench cracking. Based on a series of preliminary multi-parametric optimization tests, the following processing sequence was adopted for as-received plates, sectioned into small segments using electrical discharge machining (EDM), to promote a high fraction of special grain boundaries: (i) as-received plates were electro-discharge machined into 35 x 30 x 15 mm sections, (ii) sections were solutionized at 1175°C for 1-2 hr, followed by an air cool to room temperature to dissolve the γ' precipitates, (iii) microstructures were then grain-boundary engineered using four cycles of strain and high-temperature annealing of the single-phase alloy, specifically involving cycles of cold rolling (10% reduction in thickness per cycle) followed by a 30 min anneal at 1150°C in an air furnace, and finally (iv) a duplex aging treatment (4 hr at 843°C, followed by 8 hr at 760°C) was carried out to re-precipitate the γ' as a bimodal distribution of cuboidal precipitates.

Additionally, to compare with the as-received and grain-boundary engineered microstructures, some as-received sections from the fine-grain (GE) heat were grain-coarsened by heat-treating for 3.5 hr at 1175°C; this heat treatment led to little or no change in the grain-boundary character distribution compared to the as-received material.

Table I. Typical mechanical properties of the as-received ME3 alloy at ambient and elevated temperatures for the initially fine-grain and coarse-grain heats

Temperature (°C)	Yield strength (MPa)	Tensile strength (MPa)	Reduction in area
25 (fine)	1180	1620	26%
700 (fine)	1040	1300	18%
25 (coarse)	1150	1650	21%
700 (coarse)	980	1310	15%
800 (coarse)	900	980	12%

Large-crack propagation tests: The fatigue-crack propagation behavior of large (~8–20 mm) through-thickness cracks in the as-received, grain-boundary engineered, and coarse-grained microstructures was characterized in air at ambient (25°C) and elevated (700°C, 800°C) temperatures using 6-8 mm thick, 25.4 mm wide, compact-tension C(T) specimens for as-received microstructures, all machined in the C-R orientation, i.e., with the crack plane perpendicular to the circumferential direction and crack growth in the radial direction.

However, after grain-boundary engineering, the C(T) specimens can be considered to be in the L-T orientation, i.e., with the crack plane perpendicular to the rolling direction (L) and crack growth in the transverse direction (T). Testing was performed on computer-controlled, servo-hydraulic testing machines (MTS Systems Corp., Eden Prairie, MN), in general accordance with ASTM Standard E-647,[28] with specimens cycled under stress-intensity, K, control, at frequencies between 10 and 25 Hz (sine wave) at a load ratio (ratio of minimum to maximum loads) of $R = 0.1$. Fatigue thresholds, ΔK_{TH}, defined as the minimum stress-intensity range to yield a growth rate of 10^{-10} m/cycle, were approached using automated load-shedding at a normalized K-gradient of -0.08 mm^{-1}, as specified in the standard. Multi-sample tests were conducted to verify the effect of grain boundary engineering on the large-crack propagation behavior; specifically at least three samples were tested for each microstructural condition, and in each sample growth-rates were determined under both decreasing and increasing K conditions.

Crack-length measurements at all temperatures were determined from the unloading elastic compliance, as measured by a capacitance gauge (Model: HPT-150E-S-N2-3-B, Capacitec, MA) mounted across the notch mouth. Stress intensities were determined from the linear-elastic solutions for the C(T) geometry given in ASTM Standard E-399.[29] For all tests and conditions, the specimen thickness B, width W, and crack length a, were always large compared to the maximum plastic-zone size, estimated by $r_{y,max} \sim 1/2\pi\,(K_{max}/\sigma_y)^2$, where K_{max} is the maximum stress intensity in the fatigue cycle and σ_y is the yield strength; specifically, B, W, $a > 15r_{y,max}$, implying that plane strain, small-scale yielding conditions prevailed throughout. Results are presented in terms of the crack-growth rate per cycle, da/dN, as a function of the applied stress-intensity range, ΔK.

Stress-life (S-N) testing: In order to determine the appropriate stress level for controlling small crack initiation and propagation as well as further examine the grain-boundary engineering effect, stress-life S-N tests were first conducted on as-received (fine: $D_g \sim 1.3$ μm and coarse: $D_g \sim 15$ μm) and GB-engineered ($D_g \sim 13$ μm) microstructures with the same specimen geometry in four-point bending ($R = 0.1$, frequency = 50 Hz, 25°C).

Small-crack initiation and propagation tests: Fatigue-crack initiation and propagation tests on small surface cracks were performed at 25°C on four-point bend specimens. Specifically, samples were cycled under load control at $R = 0.1$ at frequencies between 25 and 50 Hz (sine wave). Examination of the crack-growth behavior of small cracks was conducted at ambient temperature on ~10 to 900 μm long surface cracks, initiated on the top (tension) surface of 1.8 mm thick rectangular-beam specimens (40 mm long, 2.8 mm wide), loaded in four-point bending. The four-point bending test was chosen because it provides a uniformly stressed top surface between the inner two loading points. Samples were cycled under load control, with maximum surface stress between 75 and 95% of the yield stress, σ_y, at load ratio (ratio of minimum to maximum loads) of $R = 0.1$ and at a cyclic frequency between 25 and 50 Hz (sine wave). Prior to fatigue testing, the top surfaces of the specimens were polished to a 0.05 μm finish with colloidal silica and subsequently electropolished (acetic acid: perchloric acid ~ 3:1 for 5 sec at 5V) to facilitate monitoring of the surface crack behavior.

Fatigue cracks were initiated either naturally or from artificially introduced flaws, specifically focused-ion beam (FIB) milled micro-notches and Vickers micro-hardness indents. Natural

initiation was defined in the optical microscope by the first appearance of a surface crack of length ~10-30 μm, whereupon the loads were reduced in order to monitor its growth. Micro-notches were diamond-shaped with a depth of ~20 - 50 μm; these notches were assumed to be relatively strain-free as the localized etching with FIB irradiation was achieved with a low current (starting at ~1000pA, finishing at ~100pA) Gallium ion beam). Microhardness indents of similar dimension (diagonal length ~20 μm) were also used; however, despite the surrounding residual tensile field, cracks never initiated at these indents.

Measurements of the small crack growth rates were made with periodic replication, using cellulose acetate tape softened with acetone, of loaded samples every ~3-5 x 10^4 cycles throughout the test. Corresponding crack lengths were measured from these replicas using optical microscopy, with growth rates computed from the amount of crack extension (~1-10 μm) between two discrete measurements (replicas). Stress intensities were determined from the linear-elastic solutions for surface cracks in bending.[30] A semi-elliptical crack profile, i.e., a crack depth to half-surface length ratio of $a/c \sim 2/3$, was assumed, based on experimental measurements of the shape of the crack in broken samples. Results are presented in terms of surface crack-growth rate, dc/dN, as a function of the stress-intensity range, ΔK, and are compared with our previous measurements of the growth rates of large (~8–20 mm), through-thickness cracks in the ME3 superalloy in the same microstructures.

For all tests and conditions, plane strain and small-scale yielding conditions prevailed, i.e., the specimen thickness B and width W, were always large compared to the maximum plastic-zone size, specifically, $B, W > 15r_{y,max}$.

EBSD (Electron backscattering diffraction) characterization: Electron backscatter diffraction (EBSD) provides the best method to measure the grain-boundary character and the triple-junction distributions. These measurements were made, along with the crystallographic texture, by orientation mapping of metallographically prepared specimens in a Philips XL-30S scanning electron microscope (SEM) equipped with the OIM™ software from TSL, Inc. (Draper, UT). Analysis of the EBSD data was performed using custom algorithms described in detail elsewhere.[31-34] Grain boundaries were categorized according to the CSL model and the Brandon criterion.[10,11] In all cases, the EBSD characterization was performed at the center of the sample in plane perpendicular to the rolling direction; the scanned areas were typically 1 mm square and always encompassed in excess of 2000 analyzed grain boundaries.

Numerical calculation procedures: Numerical calculations were performed to discern whether the observed crack-growth rate variations resulted from local changes in the intrinsic microstructural resistance or from fluctuations in the effective crack-driving force. For example, an explanation for the growth-rate variations could be that the local grain structure modulates variations in elastic and plastic anisotropy, thereby mediating the effective driving force for crack growth. To test this hypothesis and estimate local changes in driving force, finite-element simulations that directly incorporated the observed crack geometry and microstructure were performed. The driving force estimated from these simulations was then compared to that derived from an analytic solution to obtain a local correction or shielding factor for a given crack geometry and microstructure.

A precise solution for the local driving force around the crack front of a three-dimensional surface flaw requires extraordinary computing work and a sequence of two-dimensional

EBSD maps from serial-sectioning experiments, which was not available in this study. Accordingly, the complex three-dimensional nature of the crack path and microstructure was approximated by considering only the free-surface region under plane-stress loading. We believe that such a two-dimensional approximation is justified by examining the variation in local applied stress intensity ΔK with position along the two-dimensional crack front,[30] which reveals that the largest values of ΔK exist at the surface. The specific model comprised a two-dimensional surface slice containing an irregular crack under tensile loading, i.e., as a nominal middle-cracked tension specimen (termed the "numerical specimen"). The stress-state at the surface of the beam was then well approximated by a state of pure tension applied in the numerical model. The small crack size in relation to the beam precluded the simulation of the entire width of the beam, the demands of high mesh resolution and large sample size would result in a computationally prohibitive multi-million-element simulation. For this reason the width of the numerical specimen was fixed to be twice as long as the longest crack considered. This choice ensured that the plastic zone was well contained within the specimen, thereby simplifying J-integral calculations.

The detailed crack geometry and local microstructure were incorporated using the result of the EBSD scans and crack-growth measurements to explicitly represent the crack and grain-structure in a high-resolution finite-element mesh, shown in Fig. 1. A single-crystal plasticity constitutive description was used to account for local variations in elastic and plastic anisotropies. The crystal plasticity yield strength and hardening parameters were chosen to be consistent with the experimentally determined values for the bulk specimen. The size of the surface region that was scanned using EBSD was too small to model directly as a middle-cracked tension specimen. To remedy this, the EBSD data (or "EBSD mesh") was extended to form the numerical specimen. The extended region was modeled using a single crystal plasticity description, the elastic properties of which were derived by calculating the uncracked effective moduli of the region scanned by EBSD through direct numerical simulation under plane-stress loading. This choice eliminates, on average, the elastic mismatch between the uniform mesh region containing the high-resolution orientation data and the regions where the mesh is extended. The mismatch in plastic properties between the EBSD mesh region and the surrounding extended region was rendered benign in that the plastic zone in the cases considered was contained completely in the uniform EBSD mesh region.

The finite-element analysis was performed using the ALE3D code developed at the Lawrence Livermore National Laboratory. The EBSD data was processed and suitably averaged[35] to obtain the effective crystal orientation for each element of the mesh. The EBSD data extend over a mesh region of ~293 x 1041 μm, with a uniform element size of 1.25 x 2.15 μm. The individual crystal grains and crack geometry were resolved to a scale of ~1.6 μm, resulting on average in ~50 finite elements per grain and a crack length resolution of ~2 μm. The geometry of the crack was modeled by selectively removing material from this uniform field of crystal orientation data, resulting in a "digitized" crack geometry. The crack was primarily one element wide (1.25 μm), except in regions where the crack ran diagonally to the mesh, where it was then typically double this width. This approach was adopted to facilitate crack reconstruction at a various stages of crack growth while maintaining a consistent finite-element mesh and crystal orientation distribution. The uniform mesh region spanned by the EBSD data was not large enough to accommodate the numerical specimen of the desired size

and thus was extended both laterally and vertically to a size of 2.079 x 1.624 mm with the resulting finite-element simulation consisting of over 490,000 degrees-of-freedom.

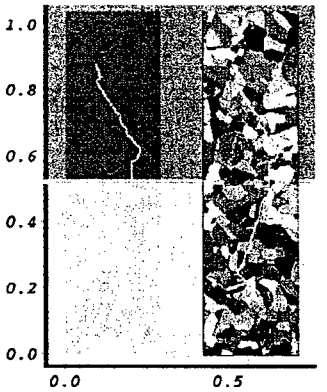

Fig. 1: Finite-element computational zones showing region of embedded crack data from the EBSD data and regions used to calculate the crack-driving forces for the both ends of the crack in the "numerical specimen" (scale in mm).

Simulations were performed corresponding to six different crack lengths (between 400-820 μm) where significant changes in the crack-growth rate were observed experimentally. A uniform tensile stress was applied such that, for the longest crack considered, the applied ΔK for a straight crack in the numerical sample was equal to that at the surface of the experimental bend beam, where the analytical solutions under conditions of small-scale yielding were used in both cases. The stress level (400 MPa) from this long-crack limit calibration was then fixed for all six simulations. This ensured that the applied K for a given crack length in the numerical specimen was comparable to the estimated value for the same crack length; in most cases, the simulated applied ΔK was within 6% of the experimentally estimated value. The simulated stress and strain fields under quasi-static loading were then used to calculate the values of the J-integral[36] for both the upper and lower cracks. The value of the J-integral (J_{FE}) calculated from the finite-element simulation was then compared to the J-integral (J_{SSY}) estimated from the analytic solution of a straight crack under the same conditions of loading under the assumptions of small-scale yielding. To facilitate comparison with experiment, the values of J_{FE} and J_{SSY} were expressed in terms of equivalent K_{FE} and K_{SSY}. The ratio of K_{FE} and K_{SSY} calculated for a given crack configuration and applied loading of the numerical specimen was then used to correct the estimate of the applied ΔK (namely, $\Delta K_{cor} = \Delta K \cdot (K_{FE} / K_{SSY})$) in the small-crack experiment corresponding to the same crack configuration and apparent loading (K_{SSY}).

Role of grain-boundary engineering on fatigue-crack propagation of large cracks

Grain-boundary characterization: The EBSD results on the grain-boundary character distribution and texture of the as-received and grain-boundary engineered microstructures are given in Fig. 2; both the fine-grain (GE) and coarse-grain (NASA) as-received and grain-boundary engineered structures are shown. In this figure, the random-grain boundary network is enhanced in black and the special grain boundaries are in color, red representing Σ3 (twin)

boundaries and yellow other $\Sigma 3^n$ special boundaries. Corresponding characteristics of all microstructures, including the grain-coarsened structure, are listed in Table II. It should be noted that, barring the grain size, the characteristics of the fine- and coarse-grained materials are essentially the same.

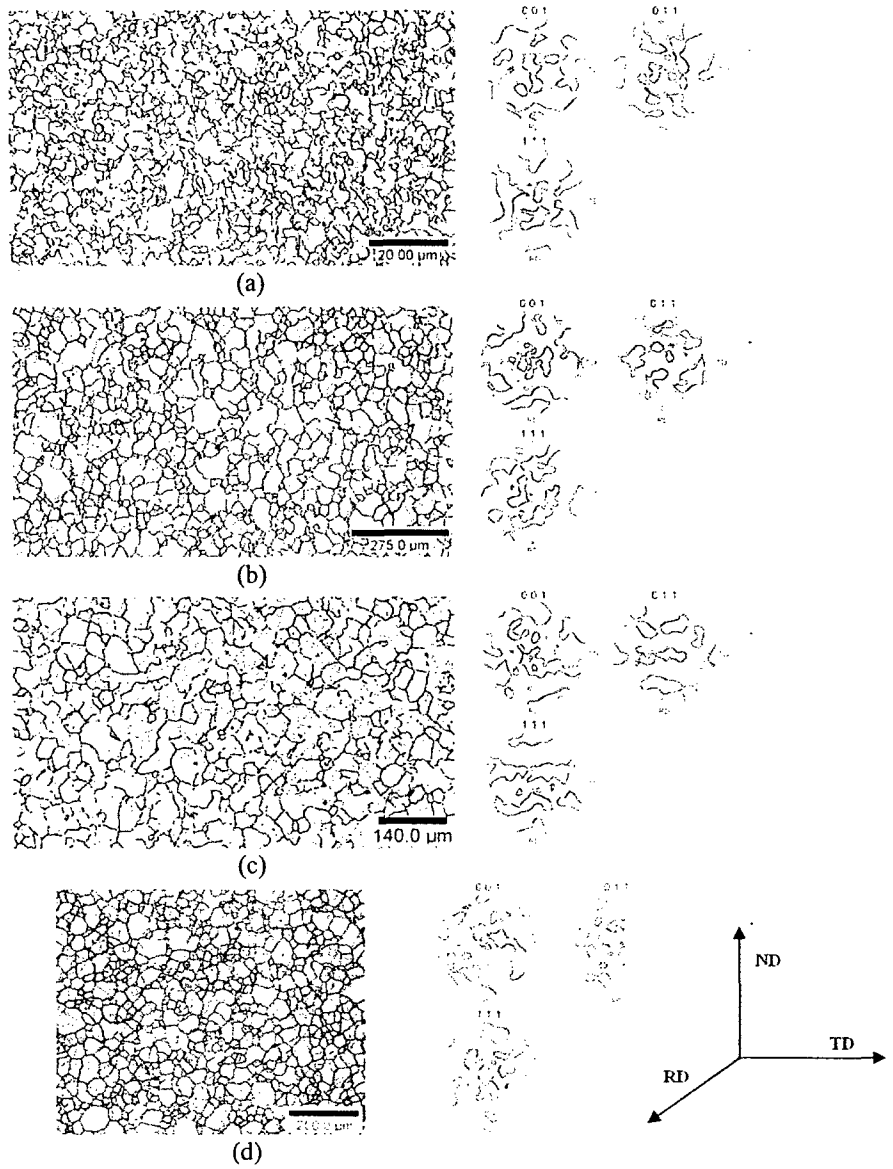

Fig. 2: Grain-boundary character distribution and texture pole figures, derived using EBSD for the ME3 alloy in the (a) as-received fine-grain (GE), (b) as-received coarse-grain (NASA), (c) grain-boundary engineered (fine-grain), (d) grain-boundary engineered (coarse-grain) conditions (for the plane perpendicular to the rolling direction). Random boundaries are shown as black lines and special boundaries are in color (red ≡ $\Sigma 3$ (twin), yellow ≡ $\Sigma 3^n$ special boundaries). The {001}, {011}, and {111} pole figures, showing the rolling (RD), transverse (TD), and normal (ND) directions, were also generated from the EBSD data.

Table II. Microstructural parameters for ME3 alloy microstructures in the as-received, grain-boundary engineered and grain-coarsened conditions

Characteristics	As-received (fine-grain)	As-received (coarse-grain)	GB-engineered (fine-grain)	GB-engineered (coarse-grain)	Grain-coarsened
Average grain size (μm)	1.3	15	13	16	17
Grain size range (μm)	0.5-6.5	4-77	3-60	5-100	4-72
Special length fraction (f_L)	0.36	0.38	0.57	0.56	0.50
Special number fraction (f_N)	0.29	0.28	0.42	0.41	0.30
Triple Junction distribution	J_0=0.32 J_1=0.51 J_2=0.13 J_3=0.04	J_0=0.34 J_1=0.51 J_2=0.12 J_3=0.03	J_0=0.17 J_1=0.56 J_2=0.12 J_3=0.15	J_0=0.16 J_1=0.56 J_2=0.11 J_3=0.17	J_0=0.27 J_1=0.57 J_2=0.10 J_3=0.06
$J_2/(1-J_3)$ [a]	0.135	0.124	0.141	0.133	0.106
Texture (× random)	1.5 (very weak)	1.6 (very weak)	1.5 (very weak)	1.7 (very weak)	1.6 (very weak)
Cluster mass (random boundary network)	90% > 1000	90% > 500	80% > 500	...	...

[a] J_n refers to the fraction of triple junctions that have n special grain boundaries

For both alloys, the (number) fraction of special grain boundaries, f_N, in the as-received condition constitutes no more than 29% of the total number of boundaries. After grain-boundary engineering, however, this "special fraction" by number was increased to 41-42%[1]. With respect to grain size, the coarse-grain alloy remained effectively unchanged after the grain-boundary engineering processing, whereas the initially fine-grain alloy showed grain coarsening from an average of 1.3 to 13 μm. Additional EBSD scans verified that these microstructures were isotropic regardless of the plane of observation.

Specifically, grain-boundary engineering resulted in an increase in the number fraction of special boundaries, from 0.29 to 0.42 and from 0.28 to 0.41 in the fine- and coarse-grain alloys, respectively. Additionally, the length fractions (f_L) of special boundaries were correspondingly increased in the two alloys from 0.36 to 0.57 and 0.38 to 0.56. The disproportionate increase in the length fraction in comparison with the number fraction (f_N) is entirely due to the increased frequency of lower energy special boundaries like annealing twins (Σ3). With an increase in the fraction of special boundaries, there was also a marked

[1] This increase in the fraction of special boundaries with grain-boundary engineering is significantly higher than that reported for other two-phase austenitic alloys.[25]

reduction in the fraction of triple junctions that are coordinated with three crystallographically random boundaries $(J_0)^2$. Accompanied by an increase in the fraction of J_3 junctions, where three special boundaries are coordinated. Indeed, the listed ratio, $J_2/(1-J_3)$, has been related to the probability of crack arrest for fracture mechanisms involving intergranular crack propagation.[31,33]

Another important effect of grain-boundary engineering was seen in the cluster mass distribution.[32,33] Over 95% of the random boundaries in the as-received microstructures were in clusters larger than 500 grain diameters, which implies that the network of random boundaries was infinite in extent. This percentage was reduced to zero in the grain-boundary engineered microstructures, indicating that an infinitely percolating network of random boundaries did not exist in the engineered microstructures, even with only a modest enhancement in the fraction of special boundaries.

All microstructures (except the as-received fine-grain alloy with D_g ~1.3 μm) revealed no change in hardness (Rockwell C ~ 44) after the grain-boundary engineering processing. Additionally, they displayed very low texture, i.e., ~1.5-1.7 times random; this can be categorized as weak to no texture but is indicative of a face-centered cubic alloy with low stacking-fault energy. Specifically, only a minimal <111> component was apparent in all as-received and grain-boundary engineered structures (Fig. 2).

Grain coarsening by annealing at 1175°C (for 3.5 hr) of the (initially) fine-grain alloy resulted in an increase in grain size from 1.3 to 17 μm, although the special grain-boundary fraction remained essentially the same as the as-received microstructure; the texture (or lack thereof) was also unchanged. It is interesting to note, however, that the length fraction of special boundaries was ~0.15 higher in the grain-coarsened structure, due to the comparatively longer twin boundaries (Σ3) in the coarser microstructure after grain growth.

Ambient-temperature fatigue-crack growth behavior: The variation in the fatigue-crack propagation rates, *da/dN*, of large (~8-20 mm), through-thickness cracks in the as-received, grain-boundary engineered and grain-coarsened microstructures in ME3 at 25°C (with R = 0.1) are shown in Fig. 3 as a function of the stress-intensity range. The most striking feature of these results is the marked influence of grain size; values of the ΔK_{th} fatigue thresholds, listed in Table III, increase linearly from 5.6 MPa√m for a 1.3 μm grain size (as-received fine-grain alloy) to 11.5 MPa√m for a 17 μm grain size (grain-coarsened alloy), as shown in Fig. 4. However, when compared at comparable grain sizes (~13-15 μm), it is clear that there is little independent effect of grain-boundary engineering on fatigue-crack propagation and threshold behavior at ambient temperatures. ΔK_{th} thresholds are comparable (within 5%) for the as-received coarse-grain (with f_N ~ 0.28) and grain-boundary engineered (with f_N ~ 0.42) structures, despite a ~50% increase in the special grain-boundary fraction; furthermore, they are ~17% higher in the grain-coarsened microstructure (where f_N ~ 0.30).

The absence of an effect of grain-boundary engineering at 25°C is consistent with the observed mechanisms of crack extension at this temperature. SEM fractography of the fatigue surfaces in the as-received and grain-boundary engineered microstructures, shown in Fig. 5a,b at near-threshold levels and in Fig. 5c,d at higher growth-rate behavior, reveal a

[2] J_n refers to the fraction of triple points that have n special boundaries, where n=0, 1, 2, or 3.

predominantly transgranular cracking mode. Typical of many superalloys with low stacking-fault energy,[26] such transgranular crack growth was highly planar and often crystallographic in character, with the facets on the fracture surfaces consistent with slip along {111} planes (Fig. 5). Indeed, the transition to this facetted, crystallographic mode occurred in both microstructures when the cyclic plastic-zone size [$r_y \sim 1/2\pi\ (\Delta K/2\sigma_y)^2$] approached the average grain size, i.e., approximately when $\Delta K < 10\text{-}12$ MPa$\sqrt{m}$. Consequently, as cracks propagated transgranularly in ME3 at ambient temperatures, it is unlikely that changing the character of the grain boundaries, by increasing the special fraction, would have a significant effect on crack-growth resistance.

Table III. Large-crack fatigue thresholds ΔK_{TH} (in MPa$\sqrt{m}$) for $R = 0.1$ at 25-800°C

Temperatures (°C)	As-received (fine-grain)	As-received (coarse-grain)	GB-engineered	Grain-coarsened
25	5.4	9.3	9.8	11.5
700	...	8.1	9.0	...
800	...	9.3	11.2	...

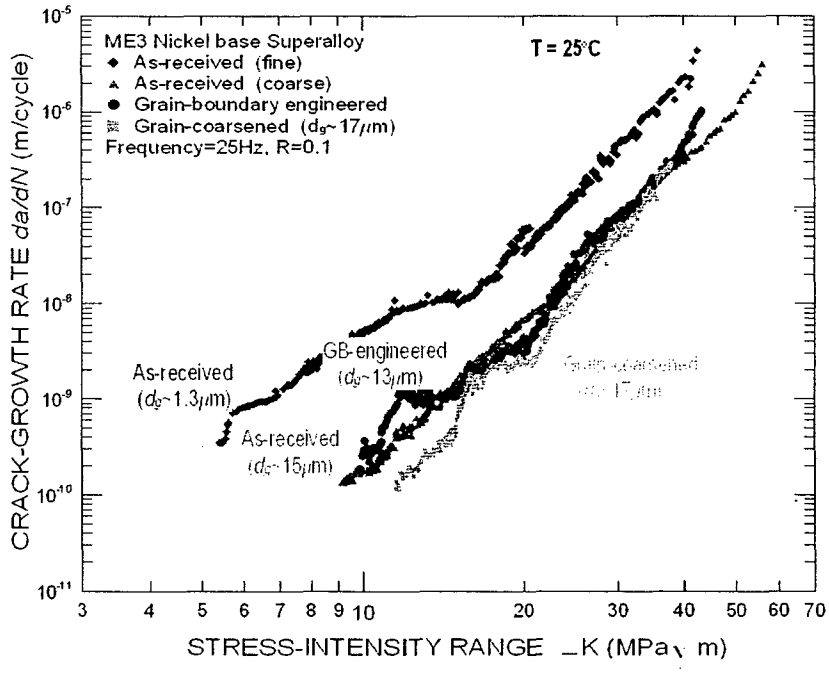

Fig. 3: Fatigue-crack propagation rates, *da/dN*, at 25°C for large (~8-20 mm) cracks in the nickel-base superalloy ME3, as a function of the stress-intensity range, ΔK, for the as-received, grain-boundary engineered and grain-coarsened microstructures. Note the large effect of grain size on near-threshold behavior.

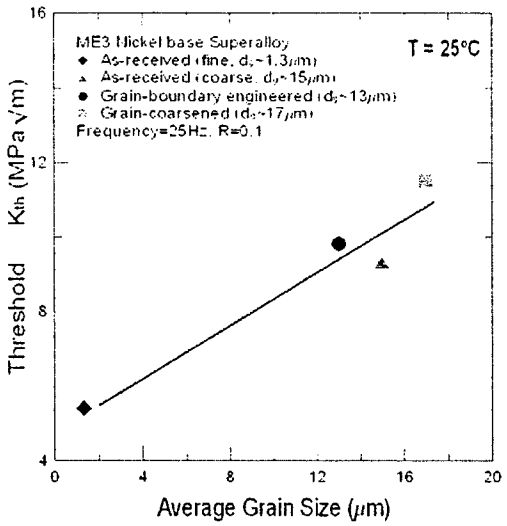

Fig. 4: Relationship between measured fatigue thresholds, ΔK_{TH}, (at R = 0.1) and the average grain size for the ME3 superalloys at ambient temperatures.

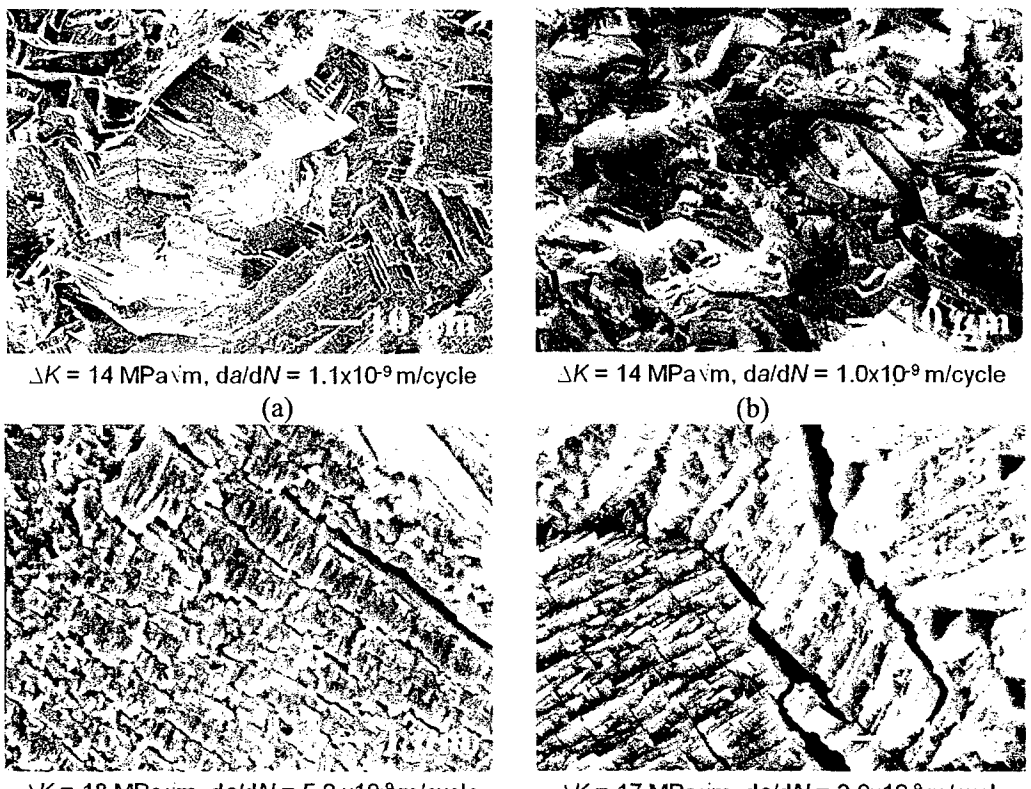

Fig. 5: SEM fractography of ambient temperature fatigue-crack propagation in ME3 at near-threshold stress intensities, for (a,c) as-received and (b,d) grain-boundary engineered microstructures.

As described below, similar results were obtained for the ambient-temperature behavior of small (~10-900 μm) surface fatigue cracks in as-received and grain-boundary engineering microstructures of ME3, where crack extension was predominantly transgranular. What is important to note here is that irrespective of the size of the cracks relative to the scale of microstructure, where the crack path is transgranular, there is little discernable effect of an increased fraction of special boundaries on the ambient temperature crack-growth resistance of fatigue-crack growth in ME3.

Elevated-temperature fatigue-crack growth behavior: To evaluate the effect of grain-boundary engineering at elevated temperatures, which are more representative of the practical applications for this alloy, large-crack fatigue-crack growth-rate data for the as-received and the grain-boundary engineered microstructures of similar average grain sizes (13-15 μm) were compared at 700° and 800°C with growth-rate data at 25°C. Results, shown in Fig. 6, indicate that crack-growth rates in both microstructures are typically faster by one to two orders of magnitude at 700°-800°C than at ambient temperature. More importantly, although there is no difference in behavior above ~10^{-7} m/cycle, there is a definitive, albeit small, increase in crack-growth resistance in the grain-boundary engineered microstructures at near-threshold levels, below ~10^{-7} m/cycle. Specifically, with the increase in fraction of special boundaries, near-threshold growth rates (at a specific ΔK) are some 5 to 10 times lower, and ΔK_{th} thresholds are ~10% higher at 700°C and over 20% higher at 800°C, as compared to values at ambient temperature (Table III).

This beneficial effect of grain-boundary engineering at elevated temperatures can also be traced to the mechanisms of cyclic crack extension. Crack path profiles at 700°C, imaged using EBSD in the SEM, show how the crack path at near-threshold levels is highly facetted, as at ambient temperatures, but now involves some intergranular crack propagation since the grain boundaries can act as preferential paths for the diffusion of oxygen and for crack advance.[35] At higher growth rates, however, crack paths cease to be facetted and revert to a fully transgranular mode (Fig. 7). This transition again occurs when the plastic-zone size becomes much larger than the grain size.

Quantitatively, the proportion of intergranular fracture could be best determined from area fractions on lower magnification SEM fractographs. As shown in Fig. 8, near-threshold fatigue-crack growth in ME3 is characterized by an increasing proportion of intergranular cracking with increase in temperature. Measurements on the as-received material at a ΔK ~ 10 MPa$\sqrt{m}$ revealed an area fraction of intergranular facets of ~40% at 700°C and as high as ~75% at 800°C. Most importantly, however, after increasing the fraction of special boundaries by grain-boundary engineering, there was a definite reduction in the relative proportion of intergranular crack growth, specifically by some 20 to 25% (Fig. 9).

Accordingly, as shown by the increase in ΔK_{th} thresholds with increasing of fraction of special grain boundaries in Fig. 10, it does appear that, due to the presence of intergranular cracking during near-threshold crack growth in ME3 at elevated temperatures (700°-800°C), there is a positive effect of grain-boundary engineering, independent of any change in grain size, in improving the resistance to fatigue-crack growth, specifically in the critical low growth-rate regime which often controls the overall life of a structure.

The precise reason why the presence of a higher fraction of special boundaries leads to a reduction in the incidence of intergranular crack growth is not known, but it seems reasonable

to presume that the effect is primarily associated with their enhanced fracture resistance, especially in the presence of a high-temperature oxidizing environment, which results in a higher proportional of transgranular cracking. Indeed, studies of environmentally-assisted intergranular cracking[13-20] and high-temperature creep[21-24] have all demonstrated the superior fracture resistance of these boundaries. However, their presence may also modify dislocation behavior, for example, by acting as a source or sink of incoming mobile dislocations. This could indirectly result in more aggregation of dislocations near the boundary, particularly as there is less free volume in special, as compared to random, boundaries, thereby strengthening the boundary region. This effect has been observed locally near individual boundaries by Alexandreanu *et al.*[37]

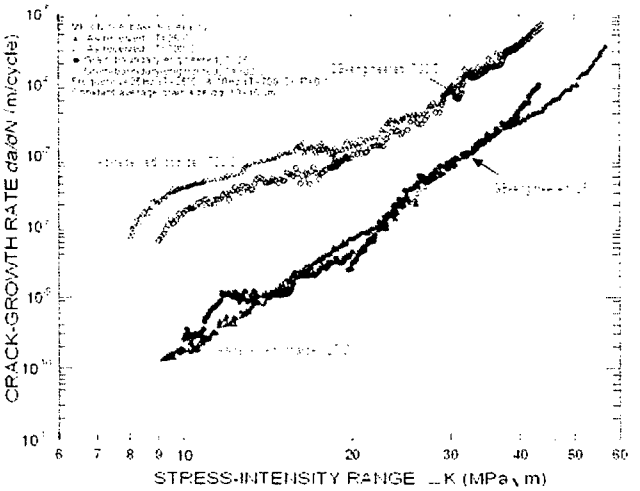

(a)

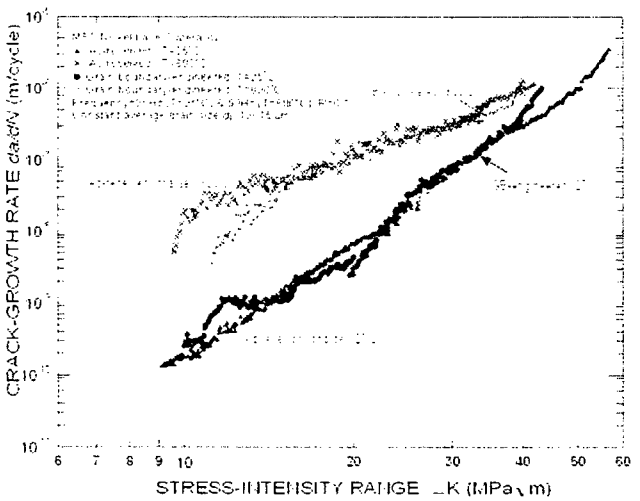

(b)

Fig. 6: Fatigue-crack propagation behavior at elevated temperatures for large (~8-20 mm) cracks in ME3, as a function of the stress-intensity range, ΔK, for in the as-received and grain-boundary engineered microstructures. Shown are results at (a) 700°C and (b) 800°C, as compared to behavior at 25°C.

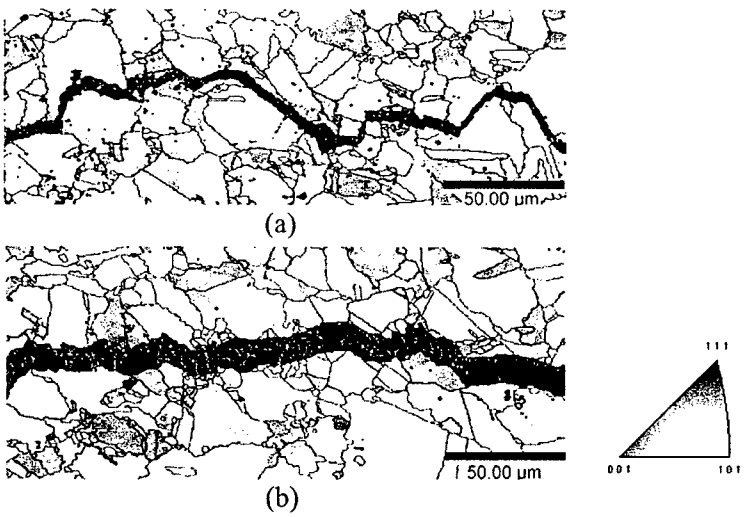

Fig. 7: EBSD maps of the fatigue-crack paths in the grain-boundary engineered ME3 microstructure tested at 700°C, showing behavior at (a) at lower growth rates (ΔK ~ 12 MPa$\sqrt{m}$) and (b) at higher growth rates (ΔK ~ 24 MPa$\sqrt{m}$). (Note that as these two micrographs were taken from the same specimen, which was cycled under decreasing ΔK conditions, the crack-opening displacement was larger for the higher growth-rate profile (b) as this region was further away (10 mm) from the crack tip when the image was taken).

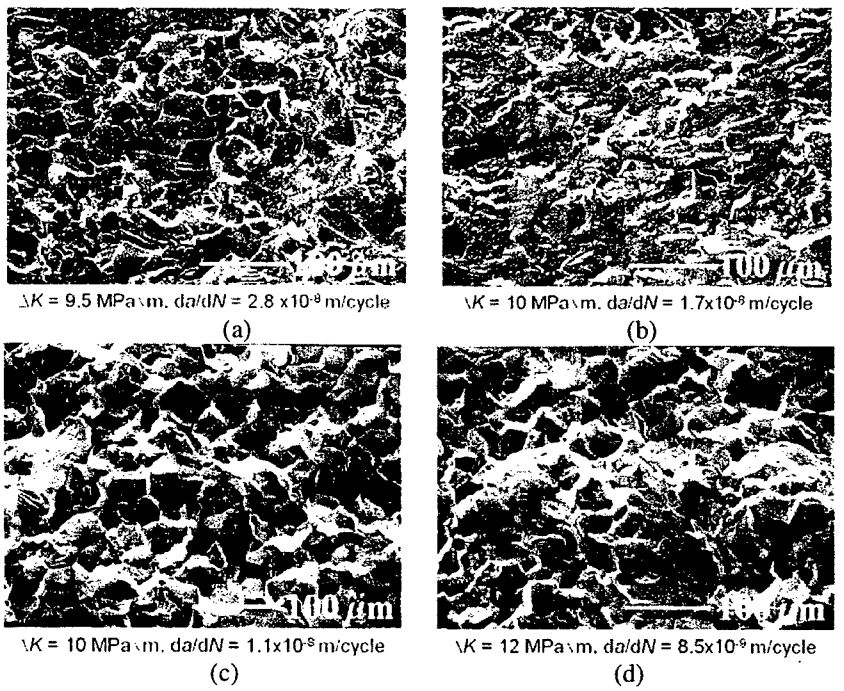

Fig. 8: SEM fractography of near-threshold fatigue-crack growth at elevated temperatures, showing a comparison between (a,c) as-received and (b,d) grain-boundary engineered microstructures (a,b) at 700°C and (c,d) at 800°C. Note the lower proportion of intergranular fracture in the engineered microstructures.

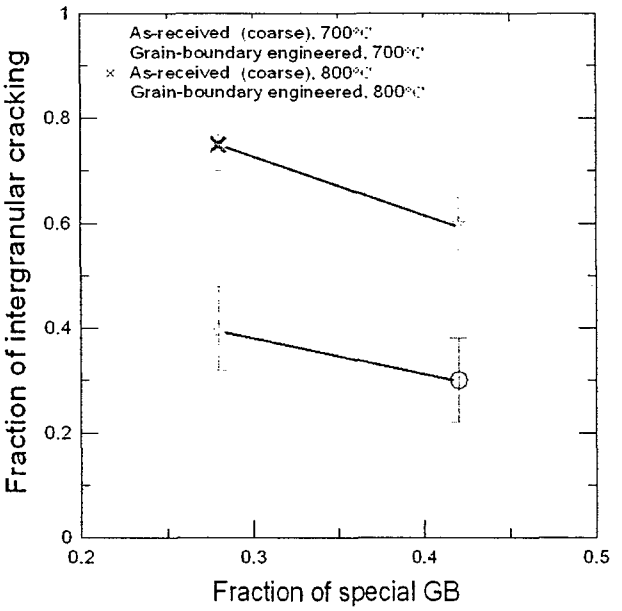

Fig. 9: Relationship between the fraction of special grain boundaries and the proportion of intergranular fracture during near-threshold fatigue-crack growth at elevated temperatures in as-received and grain-boundary engineered microstructures in ME3.

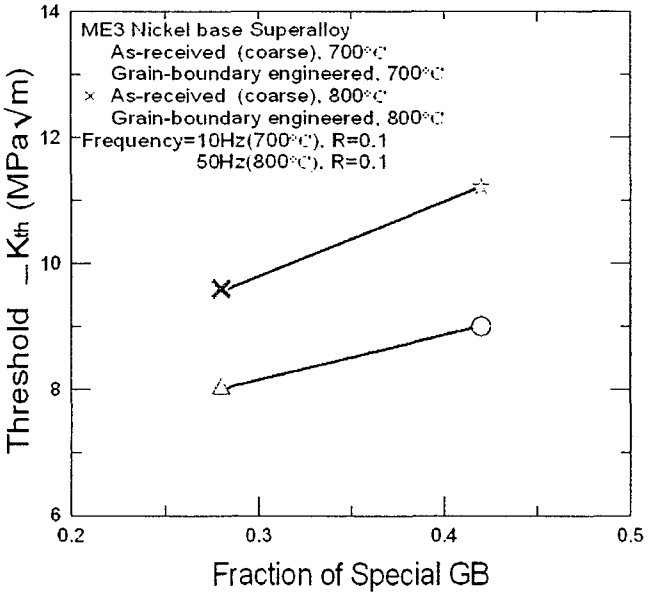

Fig. 10: Relationships between the elevated temperature ΔK_{TH} fatigue threshold in ME3 tested at 700°-800°C and fraction of special grain boundaries for the as-received and grain-boundary engineered microstructures.

In summary, using grain-boundary engineering techniques involving several cycles of strain and high-temperature annealing, the number fraction of special grain boundaries in the ME3 microstructure was increased from 28-29% to 41-42%, with little change in crystallographic texture. At constant grain size, such an increased special fraction was found to have little influence on fatigue-crack propagation and ΔK_{th} threshold behavior of large (~8-20 mm) through-thickness at ambient temperatures, primarily because crack advance in this regime is predominantly transgranular. At elevated temperatures (700-800°C), however where near-threshold fatigue-crack propagation comprises ~30 to 75% intergranular fracture, the grain-boundary engineered microstructures were found to show definitively better crack-growth resistance. Specifically, compared to ambient temperature behavior, ΔK_{th} thresholds were ~10-20% higher, and near-threshold growth rates (at a specific ΔK) were some 5 to 10 times lower in microstructures with an enhanced fraction of special grain boundaries. Such a beneficial effect on near-threshold crack-growth resistance was attributed to a ~20 to 25% reduction in the proportion of intergranular cracking in the grain-boundary engineered microstructures.

Role of grain-boundary engineering on fatigue-crack propagation of small cracks

Stress-life (S-N) behavior: The results of the stress-life (*S-N*) tests, performed in 25°C room air at $R = 0.1$, are shown for the as-received and grain-boundary engineered microstructures in Fig. 11. These data show high 10^8-cycle endurance strengths for this alloy between ~950-1050 MPa. At a nominally fixed grain size, the GB-engineered microstructure does show slightly higher (2-3%) fatigue endurance strength than the corresponding as-received microstructure. However, the most significant effect is that the finer-grained microstructure displays the superior fatigue life properties, with an endurance strength some 4 to 7% higher than that of the coarser-grained microstructures. Interestingly, this is exactly the opposite of the ranking of these microstructures when evaluated for large-crack growth resistance.

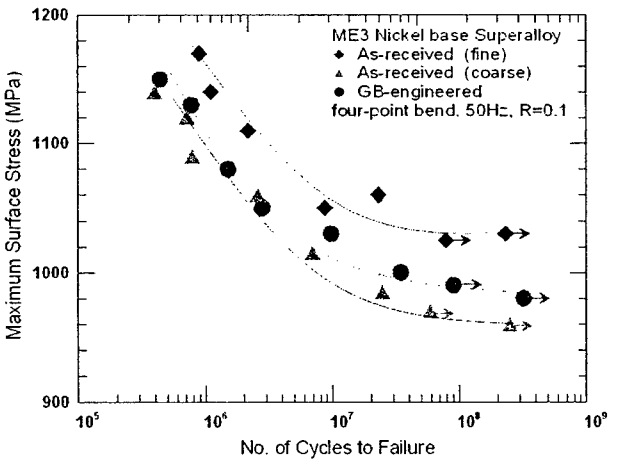

Fig. 11: Stress/life (*S/N*) curves (in 25°C room air at $R = 0.1$, 50 Hz) for the nickel-base superalloy ME3 in three microstructural conditions: as-received (fine grained: D_g ~ 1.3 μm, coarse grained: D_g ~ 15 μm) and GB-engineered (D_g ~ 13 μm).

Small-crack growth behavior: The variation in crack-growth rates of the small (~10-900 μm) surface fatigue cracks in both the as-received and grain-boundary engineered microstructures is shown as a function of the stress-intensity range, ΔK, in Fig. 12; results are compared with results for the growth of large (~8–20 mm) through-thickness cracks in the same microstructures (Fig. 3). Although small crack-growth rates are characterized by excessive scatter due to local interactions with features in the microstructure of comparable dimensions, below ΔK ~ 14 MPa$\sqrt{m}$, growth rates are definitively higher than those of equivalent large cracks and further propagate at stress-intensity ranges well below the large-crack thresholds, i.e., as low as 5-6 MPa$\sqrt{m}$. With continued propagation at higher ΔK levels ~ 18 MPa$\sqrt{m}$, large and small crack-growth rates tend to merge. However, it is apparent that similar to the behavior of large cracks, at ambient temperatures where crack advance is mostly transgranular, there is little discernable overall effect of an increased fraction of special boundaries on the growth rates of small cracks in this alloy.

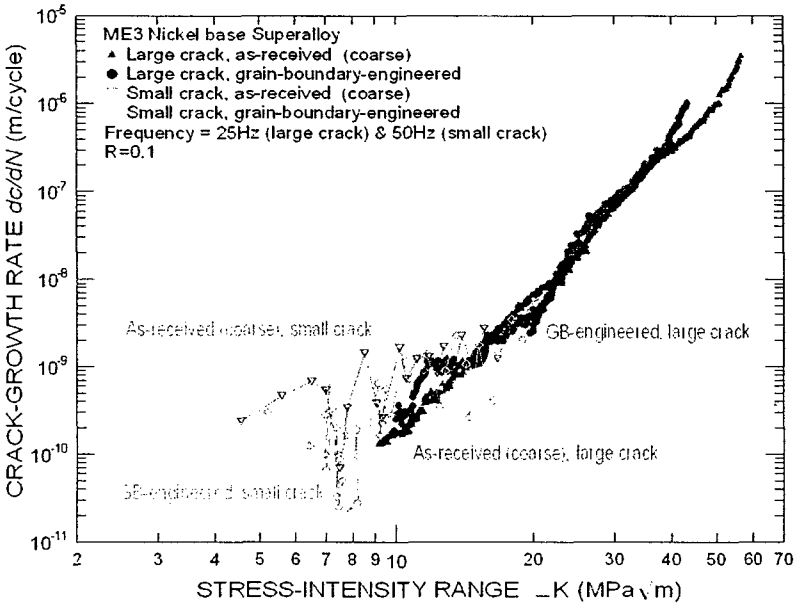

Fig. 12: Variation in fatigue-crack propagation behavior for small (~10-900 μm) surface cracks in the *as-received* (coarse-grained) and *GB-engineered* microstructures of ME3 (with approximately constant grain size of 13 – 15 μm). Testing performed in four-point bending at R = 0.1 at 50 Hz frequency in 25°C room air. Results are compared to corresponding data on the propagation of large (8-20 mm) through-thickness cracks in the same microstructures (Fig. 3).

Interaction of small cracks and boundaries of known character: To examine how such small cracks interact with individual grain boundaries of specific character, studies were performed on small (10 to 900 μm) surface cracks in the grain-coarsened microstructure (with an equiaxed matrix grain size of ~25 μm). The results of one such test are plotted in Fig. 13; here the variation in stress-intensity range and corresponding local crack-growth rates for a micronotch-initiated small crack are shown as it encounters numerous grain boundaries during cycling under a constant alternating load (the maximum surface stress was ~82% of the yield stress). Note that cracks initiated at the tips of the diamond-shaped micronotch and extended,

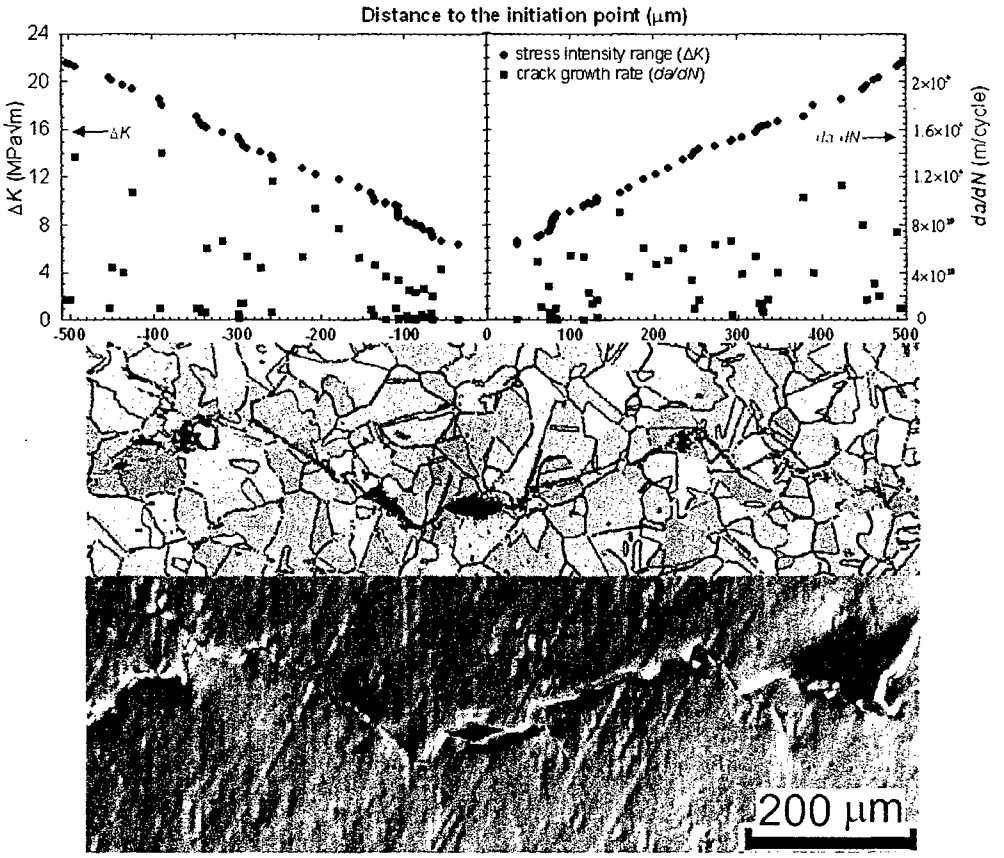

Fig. 13: Variation in fatigue-crack propagation behavior for small surface cracks in the *grain-coarsened* ME3, together with EBSD characterization of the path for small crack propagation. The crack initiated at the FIB notch at the center of the micrograph. Random boundaries are shown as black lines, twin boundaries are in red, other special boundaries are in yellow.

both left and right, along a path normal to the external cyclic loads at a nominally increasing growth rate as the ΔK values increases (with crack advance) from ~6 to 18 MPa$\sqrt{m}$. Also shown are optical micrographs of the crack and grain structure, the latter characterized using EBSD analysis to define the nature of each intercepted grain boundary; the random grain-boundary network is enhanced in yellow and the special grain boundaries are shown in red (representing $\Sigma 3$ (twin) boundaries) and blue (representing other $\Sigma 3^n$ special boundaries).

Akin to large-crack growth at ambient temperatures (Fig. 3), the surface crack path was predominantly (but not exclusively) transgranular and facetted in nature. Where the crack went intergranular (less than 10%), both random and special boundaries were sampled in approximately equal proportions. The facetted nature of the crack path can also be seen from the SEM images of the fracture surfaces in Fig. 14, where it is apparent that the tortuosity results from the crystallographic crack growth along favored slip planes in the γ matrix, and from deflection at grain boundaries due to the orientation between the adjoining grains. As expected, the crystallographic crack path was preferably along {111} planes; this is evident as the crack often extended along, or parallel to, the $\Sigma 3$ (twin) boundaries, which are

(a) (b)

Fig. 14: SEM fractographs of small-crack growth in the grain-coarsened ME3 alloy, showing the facetted nature of the crack path at the early propagation stage. Both (a) and (b) are ~200~300 μm from the crack-initiation site. (White arrows indicate the crack-propagation direction, which is normal to the externally applied stresses).

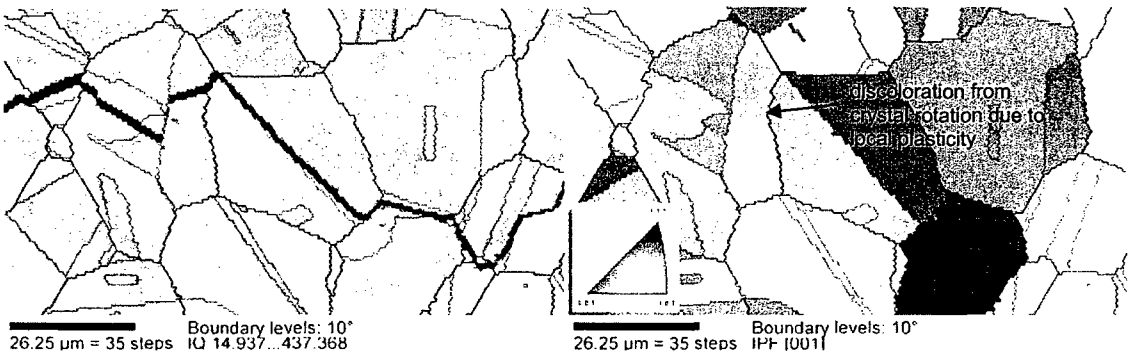

Fig. 15: EBSD images showing crystal rotation due to local plasticity as cracks impinge at grain boundaries and are then deflected crystallographic crack path is preferably along {111}, *i.e.*, crack tends to extend along, or rather close to, Σ3 twin boundaries.

invariably {111} in face-centered cubic metals (Fig. 15). Several such profiles were analyzed; some where the crack was allowed initiate naturally, as shown in Fig. 16 where crack nucleation can be seen to occur at a triple junction composed of three random grain boundaries.

To quantify how the specific boundaries, characterized by their grain-boundary misorientation angle (θ), affect the motion of the crack, further experiments of similar nature were performed. As the growing crack encountered each boundary of differing misorientation, both the crack-deflection angle ($\Delta\phi$) and change in local growth rates ($\Delta dc/dN$) were determined and an average calculated based on several measurements. Specifically, an assessment of the deflection of the transgranular crack path was made by measuring average crack-deflection angles, defined as the difference in angle between crack path before and after impingement at the boundary (as shown by the inset in Fig. 17). In addition, the perturbation

in crack-growth rate was measured, in terms of the change in growth rate at the grain boundary from the average crack-growth rate (average of 2 to 4 measurements) in the neighboring grains before and after impingement (Fig. 18). The grain-boundary misorientation angle was obtained directly from the EBSD analysis.

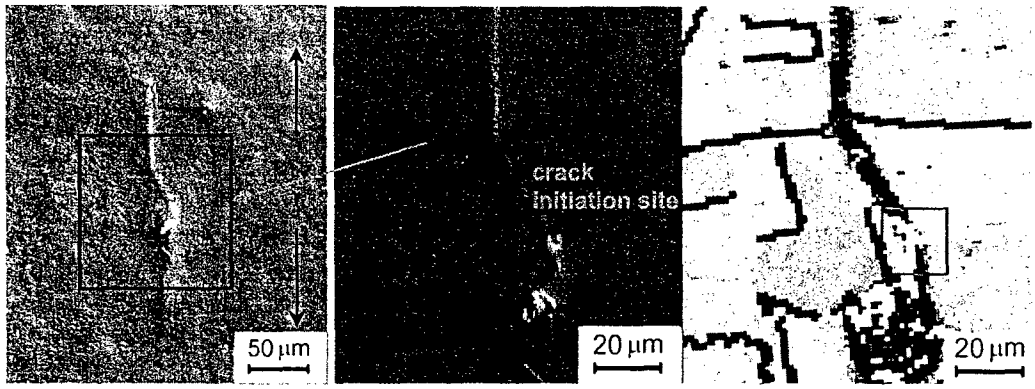

Fig. 16: Crack nucleation site in Fig. 14 showing initiation at triple junction of three random grain boundaries. (a) low-magnification and (b) higher-magnification optical microscopy images, and (c) EBSD picture showing the same crack-initiation position. Random boundaries are shown as yellow lines; twin boundaries are in red, other special boundaries are in blue. (Black arrows indicate the crack-propagation direction, which is normal to the externally applied stresses).

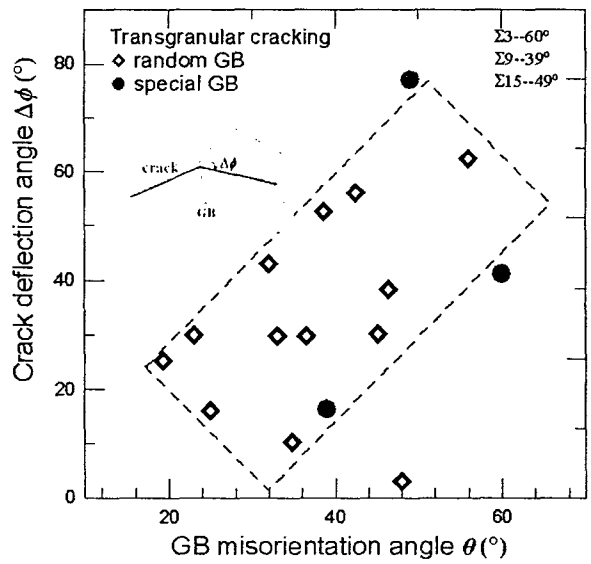

Fig. 17: Experimentally measured variation in average crack-deflection angle ($\Delta\phi$) (defined in the inset) with the grain-boundary misorientation angle (θ) for the transgranular propagation of small surface cracks as they encounter grain boundaries of known character in the grain-coarsened microstructure. A general trend of higher crack-deflection angles associated with boundaries with larger degrees of misorientation.

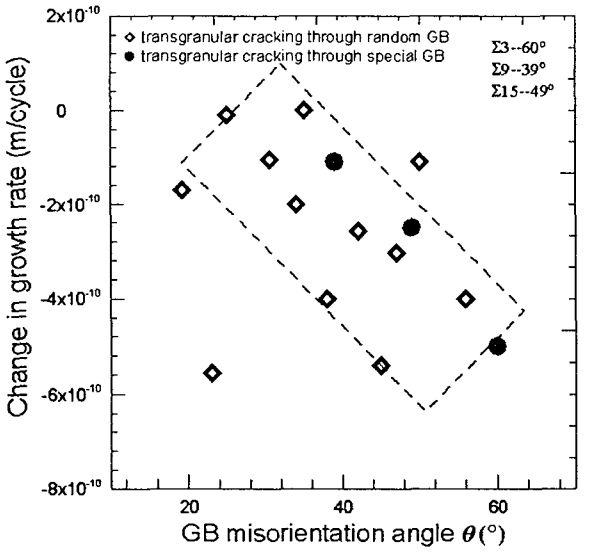

(a)

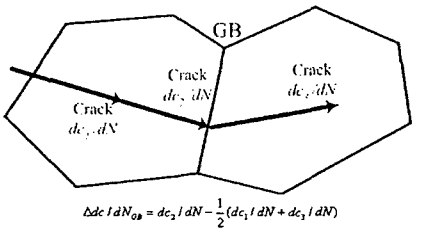

(b)

Fig. 18: (a) Experimentally measured variation in average crack-growth rates ($\Delta dc/dN$) with the grain-boundary misorientation angle (θ) for the transgranular propagation of small surface cracks as they encounter grain boundaries of known character in grain-coarsened microstructures. A general trend of higher crack-growth retardation associated with boundaries with larger misorientation angles. (b) Schematic illustrating how the change in crack-growth rates ($\Delta dc/dN$) was calculated for the process of a crack propagating through a grain boundary.

As anticipated, a general trend of higher crack-deflection angles can be seen to be associated with boundaries with larger degrees of misorientation (Fig. 17), although there is considerable scatter in the data; the behavior of special boundaries (Σ3s in this data set) does not appear to be radically different from that of random boundaries in this regard. In terms of growth rates (Fig. 18), the data suggest that grain boundaries locally retard crack extension and that special boundaries are no more effective (indeed, possibly somewhat less effective) in impeding small crack advance, although there is only a slight indication of increased retardation at random boundaries. There is, however, a general trend of increased retardation at boundaries with larger misorientation angles, with the Σ3 ($\theta \sim 60°$) twin boundaries providing some of the largest crack-growth retardations.

Finite-element calculations of local crack-driving forces: The experimental studies described above were focused on observing the growth of cracks propagating in an inhomogeneous material of varying local elastic-plastic anisotropy. To characterize this growth, a driving force (ΔK) is conventionally estimated by ignoring these local variations, on the assumption that such changes in crack geometry and material properties are both small compared to the crack size and the scale of the fracture process zone, respectively. However, it is unclear to what extent such local variations in crack geometry and elastic-plastic anisotropy affect the conventional estimates of driving force when applied to the current situation of a propagating small crack. Two-dimensional finite-element simulations that directly incorporate local geometric and material property variations into estimates of crack-driving force were performed and compared to conventional global crack estimates (from handbook stress-intensity solutions[30]) that assume idealized, geometry (straight and planar crack surface) and isotropic material parameters.

Several observations regarding the observed crack-growth rate and the corrected stress-intensity range ΔK_{cor} can be made. For a given crack length, the true driving force ΔK_{cor} at the crack tips on both sides was not same; indeed, sometimes there was a considerable difference, as much as 16% (refer to the crack length 726 μm in Table IV), as shown in Table IV (Fig. 19). Taken as a whole, there is a moderate correlation in crack-growth rate with ΔK_{cor} for the twelve cases considered (six simulations, two crack tips each). There is a strong correlation of crack-growth rate with ΔK_{cor} with the exception of the very low growth-rate data on the left side of the crack, especially the two data sets (as indicated in those connected three data points in each set shown in inset of the Fig. 19) on the right-hand side where the crack-growth rates can be well associated with corrected intensity range ΔK_{cor} and crack-deflection events (the detail of the crack-profile also shown in Fig. 13 and simulated in Fig. 20). The deflection events appear to occur when the crack tip is in the vicinity of a grain boundary and at triple junctions (Fig. 20). Although the growth rate may vary by a factor of two or so as the crack propagates across various features such as grain boundaries, it is in the neighborhood of triple junctions that gross crack deflection and an associated order of magnitude decrease in crack-growth rate are well correlated.

Table IV. Calculation of the corrected crack-propagation driving force from finite-element simulations as compared to standard analytical solutions

Crack Length	K_{FE} (left/right)	K_{SSY}	ΔK^{*}	ΔK_{cor} (left/right)**
(μm)	(MPa√m)	(MPa√m)	(MPa√m)	(MPa√m)
408	10.83/11.30	10.99	12.2	12.02/12.54
504	12.22/10.99	12.75	13.8	13.23/11.90
564	14.54/13.59	13.90	14.6	15.27/14.27
726	16.67/19.76	17.67	17.1	16.13/19.12
780	17.08/19.05	19.26	18.0	15.96/17.80
817	18.27/20.58	20.34	18.55	16.66/18.77

*determined analytically from handbook solutions.[30]

**computed for each end (left/right) of the crack using the finite-element analysis

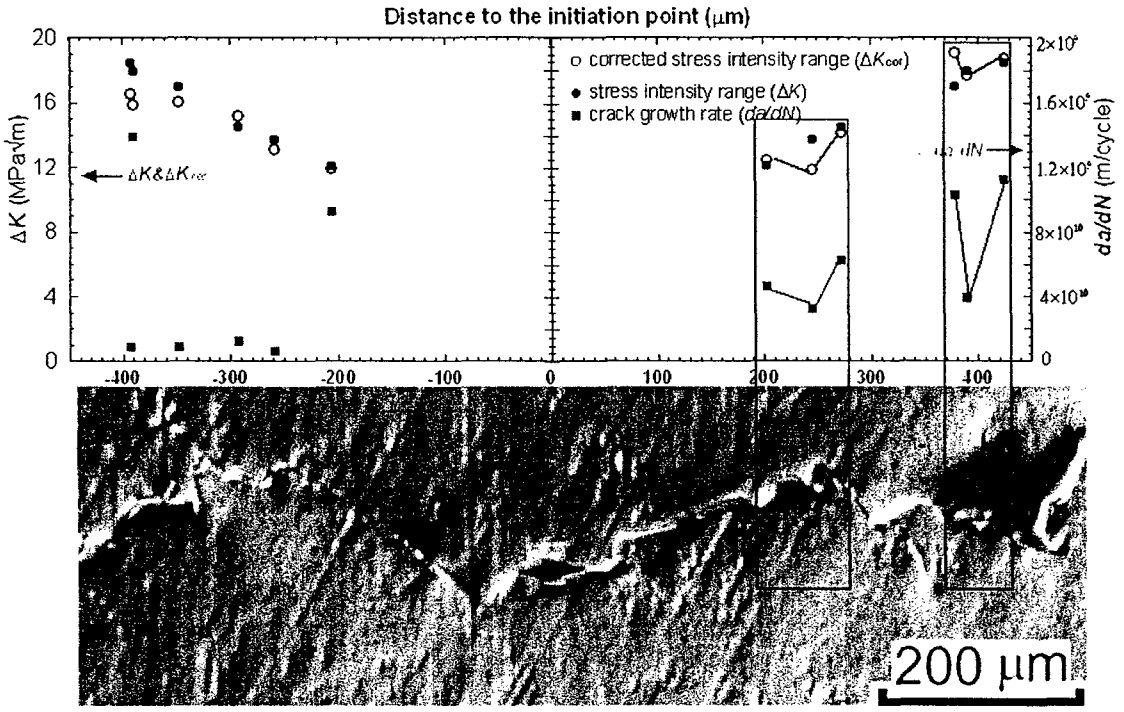

Fig. 19: Relationship between the crack-growth rate and the corrected applied ΔK_{cor}, calculated from the finite-element simulation, together with an optical microscopy characterization of the path of the small crack (similar to Fig. 13). It should be noted that there is a good correlation between measured crack-growth rates and calculated and numerically corrected stress-intensity ranges, suggesting that variations in crack-growth rate are not due to changes in driving force.

Discussion: In contrast to most studies on the effect of grain-boundary engineering on fracture, which have focused on intergranular cracking, the present work has examined how grain-boundaries affect the predominantly transgranular propagation of cracks. Specifically, the interaction of microstructurally-small cracks with boundaries of known character have been monitored in a γ/γ′ nickel-base superalloy, where the mode of crack advance is predominantly crystallographic in nature (along favored {111} slip planes).

As the crack-tip plastic-zone size for these small cracks becomes comparable to the length scale of the grain size, different misorientations across grain boundaries along the crack path, as well as the anisotropy of elastic and plastic behavior, are likely to play a key role in governing crack-growth behavior. Based on several studies on the fatigue of face-centered cubic materials,[38-40] it is known that the local crystallographic orientation of a crack can have an important effect on small crack growth. A tendency toward planar slip on the crystallographic planes, principally {111}, but also {110} and {100}, has been reported, which is confirmed by the crystallographic facets along {111} planes observed in the present study. As the boundary misorientation between adjacent grains typically contains both the tilt and twist components, this can further lead to the crack deflection and retardation. Additionally, the crack can leave a ligament when traversing a twist boundary, which can increase the retardation as it must be subsequently fractured.[38]

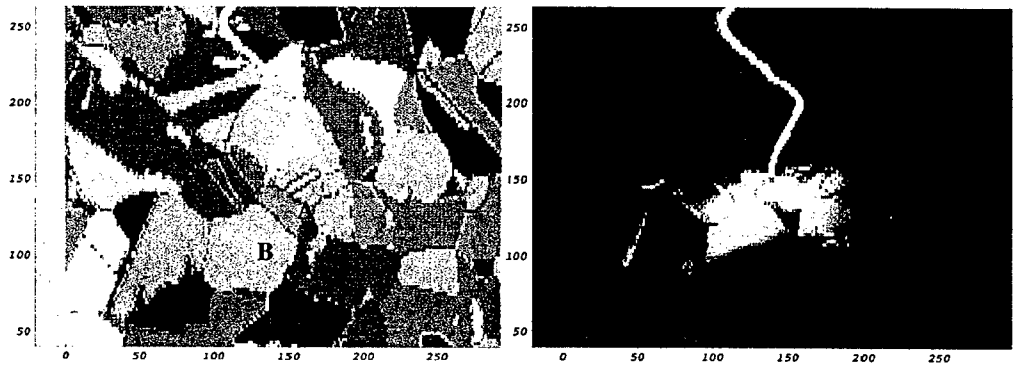

(a) crack length: 726 μm. crack-growth rate: 1.03×10^{-9} m/cycle. ΔK_{cor}: 19.1 MPa$\sqrt{m}$

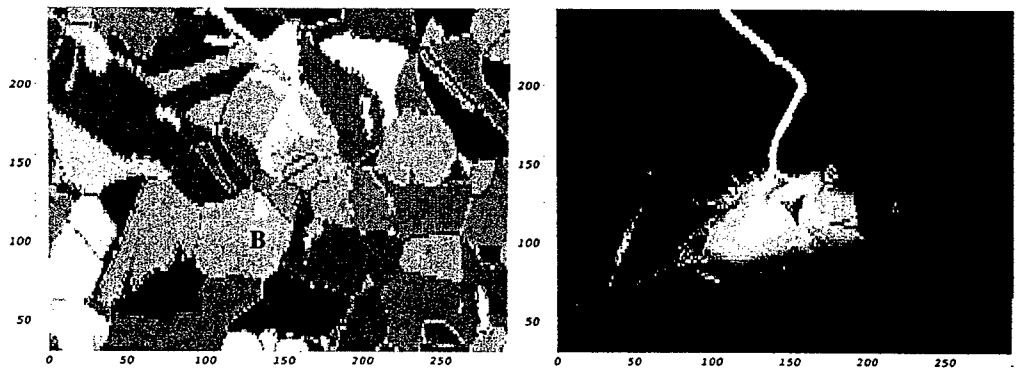

(b) crack length: 780 μm. crack-growth rate: 0.40×10^{-9} m/cycle. ΔK_{cor}: 17.8 MPa$\sqrt{m}$

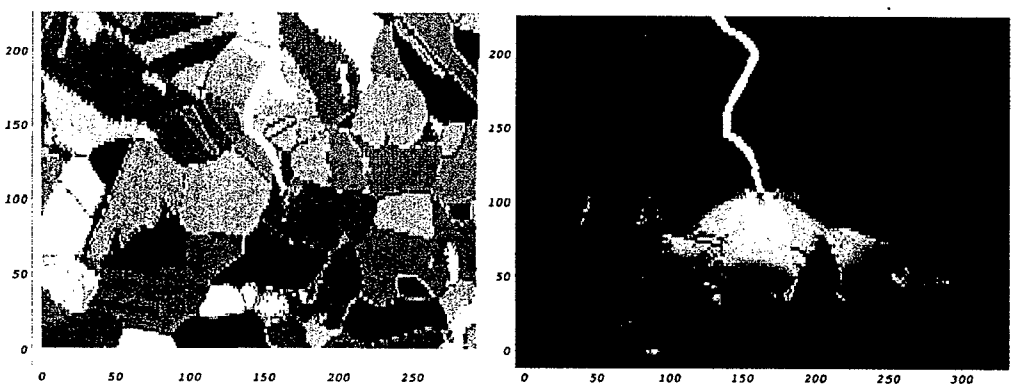

(c) crack length: 817 μm. crack-growth rate: 1.13×10^{-9} m/cycle. ΔK_{cor}: 18.8 MPa$\sqrt{m}$

Fig. 20. EBSD characterization (left) and corresponding plastic-zone profile (right) in front of the crack tip in three consecutive measurements during the small crack propagation (scale in micrometers). Of note is that where the plastic zone becomes bifurcated (e.g., in (b)), a decreased in crack-growth rate is seen. Local changes in crystal orientation in grain "A" and grain "B", predicted by the finite-element analysis, are well correlated with the EBSD data.

In the present work on small surface cracks that are propagating transgranularly and impinging on grain boundaries, our experimental studies clearly show that the degree of deflection and the magnitude of the crack-growth retardation are both increased with increase in the crystallographic misorientation across the boundary (Figs. 17-18). There is considerable scatter in the growth-rate measurements, of course, but these results do suggest that *special and random boundaries are comparable in their effect in perturbing the transgranular progress of small cracks.* Although one might think that special boundaries would be somewhat more effective as they generally have large misorientations, at fixed boundary misorientation angle our current data show that the random boundaries induce the slightly larger crack-growth retardations (Fig. 18).

However, our data also show that $\Sigma 3$ twin boundaries (where $\Delta\theta \sim 60°$) are a particularly effective means of slowing down the progress of small cracks, and this may present a reason for employing grain-boundary engineering for high-cycle fatigue resistance. We have shown for large-crack propagation that an increased fraction of special boundaries can lead to higher long-crack fatigue thresholds at elevated temperatures (700°-800°C in MP3) by acting to diminish the role of intergranular cracking. We now show that this increased special fraction, by virtue of the resultant increase in the fraction of twin boundaries, can also enhance the resistance to transgranular small crack growth, although it must be stated than quantitatively both effects are not large.

In addition to the character of the boundaries, it appears that the presence of multiple grains near the crack tip has a strong influence on the proclivity for crack deflection and the reduction of the crack-growth rate (Fig. 20). Closer examination of these finite-element results indicates that, when a crack tip resides predominantly within one grain, the plastic zone (within a 200 μm wide region where small-scale yielding holds) appears as a sharp, well-focused slip band or shear zone (Fig. 20c), which is often associated with a fast growing crack. As the crack tip approaches a triple junction, the multitude of additional slip-systems presented by adjacent grains diffuses and spreads the intensity of the plasticity, often resulting in a bifurcated or multi-branched plastic zone (Fig. 20a,b), especially in Fig. 20b where the plastic zone is much more strongly split, or bifurcated than in Fig. 20a. This stronger bias of the plastic zone to the left is considerable, even though not enough to cause the crack to change direction, but greatly reduces the advance of the right-going branch. This "virtual crack branching" may effectively lower the local crack-driving force and provide the impetuous for crack deflection, noticing that the crack-growth rate in Fig. 20b is considerably lower than those in Fig. 20a,c while the driving force ΔK_{cor} in Fig. 20b is only slightly lower.

It is interesting to observe that local crystal orientation within single grains due to the plastic deformation ahead of the crack tip are predicted by the finite-element simulation, (i.e., notice the color change in the grain "A" and "B" shown in Fig. 20b as compared to Fig. 20a.) The apparent disappearance of this region in Fig. 20c is due to the manner in which the simulations were conducted. The simulations were performed by "inserting" the crack geometry into the grain-boundary structure with subsequent monotonic loading and therefore do not capture the details of the fatigue process and crack growth. The calculations do provide an estimate of the distribution and relative intensity of the stress and plastic strain fields as modulated by the local microstructure.

In general, the variation of the local crack-driving force (ΔK_{cor}) for small cracks calculated in the finite-element simulations is on the order of 10% and can be as large as 16% when compared to the conventional stress-intensity estimate. This unaccounted variation in driving force should be considered when examining the apparent local scatter in observed crack growth rates.

Assuming Paris-law type behavior, these variations in driving force could further amplify the variability in growth rate, depending upon the value of the exponent. The variability in the observed crack-growth rate can be roughly divided into two categories: factor of two or so fluctuations ("small fluctuations") and order of magnitude variations ("large fluctuations"). The magnitudes of local changes in driving force, e.g., 5-15% variations in applied K due to microstructure, appear to be consistent with the small fluctuations in growth rates. With respect to the large fluctuations, an interesting observation is that in all cases where significant crack deflection occurred, a concomitant large fluctuation in crack-growth rate was observed. The finite-element simulations suggest that crack deflection may be related to a redistribution of the plastic-zone intensity at the crack tip. Such changes can be observed in Figs. 20a-c, where a small kinking event occurs in Fig. 20b. The crack-growth rate is first large (Fig. 20a), then smaller (Fig. 20b), and then increases again (Fig. 20c). The change in applied-K is ~6% while the change in crack-growth rate is ~280%, clearly orders of magnitude different. The finite-element simulations suggest that the local microstructure modulates the intensity of the local plastic zone, resulting in "virtual crack branching" of the nascent crack-tip, thereby reducing the effective driving force by diffusing the local plastic-strain concentration.

Summary and conclusions

Based on an experimental and numerical investigation into the feasibility of using grain-boundary engineering by strain/anneal cycling to promote the high-cycle fatigue resistance of a powder-metallurgy polycrystalline nickel-base superalloy René 104 (ME3) at ambient to elevated temperatures (25 to 800°C), the following conclusions can be made:

(1) Using grain-boundary engineering techniques involving several cycles of strain (10% cold rolling) and high-temperature annealing (1150°C, 30 mins), the number fraction of special grain boundaries in the ME3 microstructure could be increased from 28-29% to 41-42%, with little change in crystallographic texture.

(2) At a constant grain size, the effect of such an increase in fraction of special boundaries, however, was found to have little influence on the fatigue-crack propagation and ΔK_{th} threshold behavior of large (~8-20 mm) through-thickness at ambient temperatures, primarily because crack advance in this regime is predominantly transgranular. Fatigue thresholds and near-threshold growth rates, however, were markedly affected by grain size (~1-17 μm), with the coarser microstructures displaying significantly better fatigue-crack growth resistance.

(3) At elevated temperatures (700-800°C), where near-threshold fatigue-crack propagation comprises ~30 to 75% intergranular fracture, the grain-boundary engineered microstructures were found to show definitively better (large-crack) crack-growth resistance. Specifically, compared to ambient temperature behavior, ΔK_{th} thresholds were

~10-20% higher, and near-threshold growth rates (at a specific ΔK) were some 5 to 10 times lower in microstructures with an enhanced fraction of special grain boundaries. Such a beneficial effect on near-threshold crack-growth resistance was attributed to a ~20 to 25% reduction in the proportion of intergranular cracking in the grain-boundary engineered microstructures.

(4) Grain-boundary engineered microstructures displayed only a marginal (~2-3%) increase in 10^8-cycle endurance strength when compared at similar grain size. Fine-grained (1.3 μm) as-received microstructures, however, displayed a larger (~7%) increase in endurance strength when compared to coarse-grained (15 μm) as-received structures.

(5) Measured fatigue thresholds for small (~10-900 μm) surface cracks were considerably lower (~5 MPa$\sqrt{m}$) than those for corresponding large (8-20 mm) through-thickness cracks. However, with respect to the role of grain-boundary engineering, there was little discernable overall effect of an increased fraction of special boundaries on the growth rate and threshold behavior of these small cracks.

(6) Grain boundaries were found to provide an impedance to the predominantly transgranular propagation of small surface cracks. Specifically, boundaries with higher misorientations on average caused larger crack deflections and resulted in larger crack-growth retardations. However, at a fixed grain-boundary misorientation angle, special boundaries were no more effective than random boundaries in impeding transgranular small crack growth.

(7) Due to their large misorientations ($\Delta\theta \sim 60°$), $\Sigma 3$ twin boundaries were found to be particular effective at locally retarding such small crack extension.

(8) Corresponding numerical simulations of such small-crack growth suggest that these measured perturbations in crack-growth rates are well associated with fluctuations in the effective crack-driving force and the profile of the plastic zone near the crack tip, which is significantly affected by the local microstructure, in particular the presence of grain boundaries and triple junctions.

Acknowledgement/Disclaimer

This work was sponsored by the U.S. Air Force Office of Scientific Research, under Grant F49620-02-1-0010. Part of this work was performed by the Lawrence Livermore National Laboratory under the auspices of the U.S. Department of Energy (contract No. W-7405-Eng-48). The views and conclusions contained herein are those of the authors and should not be interpreted as necessarily representing the official policies or endorsements, either expressed or implied, of AFOSR or the U.S. Government. Thanks are due to Dr. James Stölken of the Lawrence Livermore National Laboratory for his work on the numerical simulations.

References

1. *Report of the Ad Hoc Committee on Air Force Jet Engine Manufacturing and Production Processes* 1992, The Pentagon, Air Force Scientific Advisory Board, SAF/QQS.
2. B. A. Cowles: *Int. J. Fract.*, 1996, vol. 80, pp. 147-63.

3. J. Henderson, ed.: *Proceedings of the Third, Fourth, Fifth and Sixth National Turbine Engine High Cycle Fatigue Conferences* 1998-2001, Universal Tech. Corp., Dayton, OH.
4. T. Nicholas and J.R. Zuiker: *Int. J. Fract.*, 1996, vol. 80, pp. 219-35.
5. R. O. Ritchie, D. L. Davidson, B. L. Boyce, J. P. Campbell, and O. Roder: *Fat. Fract. Eng. Mat. Struct.*, 1999, vol. 22, pp. 621-31.
6. S.A. Padula, A. Shyam, R.O. Ritchie and W.W. Milligan: *Int. J. Fat.*, 1999, vol. 21, pp. 725-31.
7. R.K. Nalla, B.L. Boyce, J.P. Campbell, J.O. Peters, and R.O. Ritchie: *Metall. Mater. Trans. A*, 2002, vol. 33A, pp. 899-918.
8. A.E. Giannakopoulos, T.C. Lindley and S. Suresh: *Acta Mater.*, 1998, vol. 46, pp. 2955-68.
9. T. Watanabe: *Res Mech.*, 1984, vol. 11, pp. 47–84.
10. H. Grimmer, W. Bollmann, and D.H. Warrington: *Acta Crystallogr. A*, 1974, vol. 30A, pp. 197-207.
11. D.G. Brandon, B. Ralph, S. Ranganathan and M.S. Wald: *Acta Metall.*, 1964, vol.12, pp. 813-21.
12. M. Kumar, A. Schwartz, and W. King: *Acta Mater.*, 2002, vol. 50, pp. 2599-612.
13. B. Bennett and H. Pickering: *Metall. Mater. Trans. A*, 1987, vol. 18A, pp. 1117-24.
14. G. Palumbo and K. T. Aust: *Scripta Metall.*, 1988, vol. 22, pp. 847-52.
15. G. Palumbo and K.T. Aust: *Acta Metall. Mater.*, 1990, vol. 38, pp. 2343-52.
16. G. Palumbo, P.J. King, K.T. Aust, U. Erb, and P.C. Lichtenberger: *Scripta Metall. Mater.*, 1991, vol. 25, pp. 1775-80.
17. D.C. Crawford and G.S. Was: *Metall. Trans. A*, 1992, vol. 23A, pp. 1195-1206.
18. P. Lin, G. Palumbo, U. Erb, and K.T. Aust: *Scripta Metall. Mater.*, 1995, vol. 33, pp. 1387-92.
19. G. Palumbo and K.T. Aust: *Canadian Metall. Quart.*, 1995, vol. 34, pp 165-73.
20. E.M. Lehockey, G. Palumbo, P. Lin, and A. M. Brennenstuhl: *Metall. Mater. Trans.*, 1998, vol. 29A, pp. 387-96.
21. J. Don and S. Majumdar: *Acta Metall.*, 1986, vol. 34, pp. 961-67.
22. D.P. Field and B.L. Adams: *Acta Metall. Mater.*, 1992, vol. 40, pp 1145-57.
23. V. Thaveeprungsriporn and G.S. Was: *Metall. Mater. Trans. A*, 1997, vol. 28A, pp. 2101-12.
24. E.M. Lehockey, G. Palumbo, P. Lin, and A. M. Brennenstuhl: *Scripta Mater.*, 1997, vol. 36, pp. 1211-18.
25. E.M. Lehockey, G. Palumbo and P. Lin: *Metall. Mater. Trans.*, 1998, vol. 29A, pp. 3069-79.
26. E. Nembach and G. Neite: *Prog. Mater. Sci.*, 1985, vol. 29, pp. 177-319.
27. T. Gabb, J. Telesman, P. Kantzos, and K. O'Connor: *NASA TM-2002-211796*, 2002.
28. ASTM, *Annual Book of ASTM Standards*, E647, American Society for Testing and Materials, West Conshohocken, PA, 2001.
29. ASTM, *Annual Book of ASTM Standards*, E399, American Society for Testing and Materials, West Conshohocken, PA, 1997.
30. J.C. Newman, and I.S. Raju: *Eng. Fract. Mech.*, 1981, vol. 15, p.185.
31. M. Kumar, W. King, and A. Schwartz: *Acta Mater.*, 2000, vol. 48, pp. 2081-91.
32. A. Schwartz, M. Kumar, and W. King: *MRS Symposium Proceedings*, 2000, vol. 586, p. 3.
33. C.A. Schuh, M. Kumar, and W. King: *Acta Mater.* 2003, vol. 51, pp. 687-700.
34. C.A. Schuh, M. Kumar, W.E. King: *Zeitschrift fur Metallkunde*, 2003, vol. 94, pp. 323-28.

35. J.H. Cho, A.D. Rollett, and K.H. Oh: *Metall. Mater. Trans A*, 2005, vol. 36, p. 3427.
36. Y. Lei: *Eng. Fract. Mech.*, 2005, vol. 72, p. 577.
37. B. Alexandreanu, B.H. Sencer, V. Thaveeprunsriporn, and G. Was: *Acta Mater.*, 2003, vol. 51, pp. 3831-48.
38. A. Gourgues: *Mater. Sci. Tech.*, 2002, vol. 18, p. 119.
39. G.G. Garrett and J.F. Knott: *Acta. Metall.*, 1975, vol. 23, p. 841.
40. P. Peralta, R. Kickerson, N. Dellan, K. Komandur, and M.A. Jameel: *J. Eng. Mater. Tech.*, 2005, vol. 18, p. 119.

Personnel Supported

Robert O. Ritchie	PI, Professor, University of California at Berkeley
Mukul Kumar	Co-PI, Lawrence Livermore National Laboratory
Yong Gao	Graduate Student, University of California at Berkeley (Ph.D. awarded May 2006)

Publications and Presentations

Degree theses:

- Yong Gao: "A study on the role of grain-boundary engineering in promoting high-cycle fatigue resistance and improving reliability in Nickel-base superalloys for propulsion systems", *Ph.D. thesis*, Department of Materials Science and Engineering, University of California, Berkeley, May 2006 (advisor: R. O. Ritchie)

Archival journal publications:

- I. Altenberger, E. A. Stach, G. Liu, R. K. Nalla, and R. O. Ritchie, "An *In Situ* Study of the Thermal Stability of Near-Surface Microstructures Induced by Deep Rolling and Laser-Shock Peening", *Scripta Materialia*, vol. 48, June 2003, pp. 1593-1598.
- I. Altenberger, R. K. Nalla, U. Noster, G. Liu, B. Scholtes and R. O. Ritchie, "Residual stress stability and near-surface microstructures in high temperature fatigued mechanically surface treated Ti-6Al-4V)", *Materialwissenschaft und Werkstofftechnik*, vol. 34, 2003, pp. 529-541.
- R. K. Nalla, I. Altenberger, U. Noster, G. Y. Liu, B. Scholtes, and R. O. Ritchie, "On the Influence of Mechanical Surface Treatments – Deep Rolling and Laser Shock Peening – on the Fatigue Behavior of Ti-6Al-4V at Ambient and Elevated Temperatures", *Materials Science and Engineering A*, vol. 355, 2003, pp. 216-230.
- Y. Gao, M. Kumar, R. K. Nalla, and R. O. Ritchie, "High-Cycle Fatigue of a Nickel-Base Superalloy ME3 at Ambient and Elevated Temperatures: Role of Grain-Boundary Engineering", *Metallurgical and Materials Transactions A*, vol. 36A, 2005, pp. 3325-3333.
- Y. Gao, J. Stölken, M. Kumar, and R. O. Ritchie, "High-Cycle Fatigue of Nickel-Base Superalloy René 104 (ME3): Interaction of Microstructurally-Small Cracks with Grain Boundaries of Known Character", *Acta Materialia*, 2006, in review.

Conference publications:

- I. Altenberger, R. K. Nalla, U. Noster, G. Liu, B. Scholtes and R. O. Ritchie, "Effects of Deep Rolling on the Fatigue Behavior of Ti-6Al-4V at Ambient and Elevated Temperatures", *Proc. 10th World Cong. on Titanium – 2003, G. Lütjering, ed.,* Wiley-VCH, Weinheim, Germany, 2003.

Conference presentations:

- I. Altenberger, R. K. Nalla, U. Noster, B. Scholtes, and R. O. Ritchie, "On the Effects of Residual Stresses on Fatigue Behavior in Ti-6Al-4V", invited presentation at the Symposium on *Measurement and Interpretation of Internal/Residual Stresses,* TMS Annual Meeting, San Diego, CA, 2003.
- I. Altenberger, U. Noster, R. K. Nalla, B. Scholtes, and R. O. Ritchie, "Residual Stress Relaxation in Fatigue of Mechanically Surface Treated Materials", presented at the Symposium on *Measurement and Interpretation of Internal/Residual Stresses,* TMS Annual Meeting, San Diego, CA, 2003.
- M. Kumar was an invited speaker at the *Gordon Research Conference on Physical Metallurgy (Interfaces),* Holderness School, NH, July 2002; TMS Annual Meeting 2004, Symposium on "The Role of Grain Boundaries in Materials Design," Charlotte, NC (March 2004); organized symposium titled "Interfacial Engineering for Optimized Properties," MRS Spring Meeting, San Francisco, CA (April 2004).
- Y. Gao, M. Kumar, and R. O. Ritchie, "Propagation of Small Surface Cracks in Nickel-Base Superalloy ME3", presented at the Symposium on *Fatigue and Fracture of Traditional and Advanced Materials,* at *TMS 2006,* 135th TMS Annual Meeting, San Antonio, TX, 2006.

Awards Received

R. O. Ritchie was elected to the National Academy of Engineering in 2001, and the Royal Academy of Engineering, London in 2002; in addition, he was made a TMS Fellow, was the ASTM Annual Fatigue Lecturer, and won the Nadai Award from ASME in 2004 and the Wöhler Medal from the European Structural Integrity Society in 2006.

Transitions

M. Kumar and R. O. Ritchie have maintained close interactions with GE Aircraft Engines and NASA Glenn, as these organizations provided the ME3 disk alloy used in this research.